JOURNAL OF SOLID STATE CHEMISTRY 69, 116–125 (1987)

New Silica-Containing Ferrite Phases in the System $NaFeO_2$–SiO_2

I. E. GREY AND C. LI

CSIRO, Division of Mineral Chemistry, P.O. Box 124, Port Melbourne, Victoria, Australia 3207

Received July 30, 1986

Phase equilibria on the pseudobinary join $NaFeO_2$–SiO_2 have been determined for SiO_2 contents in the range 0–20 mole% and for temperatures in the range of 700–1350°C, using thermal analysis methods and high-temperature X-ray diffraction. A new cubic polymorph, δ-$NaFeO_2$, has been found to be stable from 1250°C up to the melting point. The δ-phase forms solid solutions with SiO_2, extending over the full composition range studied. The lower-temperature γ and β polymorphs of $NaFeO_2$ form limited solid solutions with SiO_2, containing up to 5 and 11 mole% SiO_2, respectively. A new solid solution, γ'_{ss}, was identified with a lower SiO_2 composition limit of 7.5 mole%, at 1050°C, that extends beyond the upper SiO_2 content considered in this study. The γ'_{ss} members have orthorhombic symmetry with unit cell parameters $a_{\gamma'} \simeq a_\gamma$, $b_{\gamma'} \simeq 2b_\gamma$, $c_{\gamma'} \simeq 2c_\gamma$. X-ray diffraction data are given for the various silica-containing ferrite phases as a function of temperature and SiO_2 content, and a new mechanism is proposed for the β to γ structure transformation. The applicability of the results to a new process for regeneration of spent paper-pulp liquors is discussed.

Introduction

A new process has been recently developed for caustic (NaOH) regeneration from spent paper pulp liquors (*1*). It is called the DARS process (Direct Alkali Recovery System) and it involves reaction of the spent liquor with hematite in a fluid-bed roaster at 900–1000°C to form beta sodium ferrite, β-$NaFeO_2$. The roast product is hydrolyzed in hot water to produce NaOH solution and solid iron oxide which is recycled to the roaster. Associated Pulp and Paper Mills (APPM) have constructed the first commercial-scale DARS process in their Burnie (Tasmania) mill (*2*). In laboratory testing of the process at APPM, the phenomenon of retention of hydrolysis-resistant sodium in the recycled iron oxide was observed. A collaborative project was established with CSIRO to investigate the causes of sodium retention.

Application of X-ray diffraction (XRD) and scanning electron microscopy (SEM) to roast and hydrolysis samples revealed the presence of a new, hydrolysis-resistant, ferrite phase that was stabilized by silica impurities in the hematite. Microprobe analyses showed that the new phase had an extended composition range along the $NaFeO_2$–SiO_2 join, with silica contents in the approximate range 10–30 mole%. The discovery of the new ferrite led to a general investigation of the influence of silica on the stability and phase relations of sodium ferrite. We report here the results of a

0022-4596/87 $3.00

study on the system $NaFeO_2$–SiO_2 for temperatures in the range 700–1350°C and for silica contents in the range 0–20 mole%.

There is little information in the literature relevant to the $NaFeO_2$–SiO_2 join. Bowen, Schairer, and von Willems reported a compound of molar composition $6Na_2O$–$4Fe_2O_3$–$5SiO_2$, which lies close to the pseudobinary join (*3*). However, later studies at 700°C by Collins and Mulay (*4*) showed no evidence of the 6–4–5 phase, or any other ternary compounds in the region of the Na_2O–Fe_2O_3–SiO_2 system bounded by Na_2O–Na_2SiO_3–Fe_2O_3 (which includes the pseudobinary join between $NaFeO_2$ and $NaFeO_2 \cdot 0.5SiO_2$).

The end-member composition, $NaFeO_2$, occurs in three polymorphic modifications designated as α, β, and γ in order of increasing temperature of the stability range. The α form, stable below 760°C, has rhombohedral symmetry, $R\bar{3}m$. It has a rock salt superstructure with both iron and sodium in octahedral coordination (*5*). The β form of $NaFeO_2$ is stable between 760° and 1010°C (*6, 7*). It has orthorhombic symmetry, $Pna2_1$, with an ordered wurtzite superstructure, in which Na and Fe atoms are ordered over one set of tetrahedral sites within a hexagonal close-packed array of oxygens. At 1010°C, β-$NaFeO_2$ transforms reversibly to the γ form. Its structure has not been determined, but by analogy with γ-$NaAlO_2$, with which it forms extensive solid solutions, it is presumed to have tetragonal symmetry, $P4_12_12$, with ordering of Na and Fe atoms in the tetrahedral sites of a tetragonal packing of oxygen atoms (*8, 9*). There is a close structural relationship between the β and γ forms. A topotactic transformation involving a movement of half the cations from filled to empty tetrahedral sites has been proposed (*10*). Alternatively, the transformation can be described in terms of rotations of some of the FeO_4 tetrahedra, which involves breaking and reforming Na–O bonds only, as will be described in this paper.

Experimental

The starting materials used were Fisher certified Fe_2O_3, BDH analytical-grade sodium oxalate, and BDH laboratory reagent precipitated silica. The first two samples were dried at 600° and 100°C respectively and kept in a desiccator. The water content of the precipitated silica was determined by measuring the weight loss on firing to constant weight at 900°C.

Mixtures were obtained by weighing and grinding the three reagents in the molar ratios $Na_2O : Fe_2O_3 : ySiO_2$, with y at 0.025 increments from 0 to 0.20 and at 0.05 increments from 0.20 to 0.50. The sample mixtures were contained in platinum crucibles and heated in air overnight at 800°C, then reground and heated for 4 hr at 1000°C. The samples were stored in a vacuum desiccator before use.

The prereacted compositions were used for phase diagram studies in the temperature range 700° to 1350°C. The liquidus and solidus lines and the subsolidus phase boundaries were established using differential thermal analysis (DTA) coupled with high-temperature X-ray diffraction. The DTA measurements were made using a Stanton Redcroft STA-780 thermal analyzer. About 10 mg of the samples were heated in a static atmosphere at rates of 10° and 50°C min^{-1}, using hematite as reference material. The higher heating rate gave better definition of the weaker, broader thermal effects.

The phases in the reaction products were identified from powder patterns taken with a Philips diffractometer fitted with a graphite monochromator and employing CuK_α radiation. For lattice parameter determinations, silicon was added as an internal standard. The study of phases that could not be preserved by quenching and the variation

of lattice parameters with temperature was made using a Rigaku theta–theta high-temperature diffractometer, with automatic temperature programmer. The sample was contained within a depression in the Pt/Rh strip heater and the temperature was recorded using a Pt, Pt/13% Rh thermocouple welded onto the base of the sample cavity. At each new temperature setting the position of the strip heater was adjusted, to coincide with the diffraction plane of the diffractometer, using a fluorescent screen and the direct X-ray beam.

For one of the silica-containing ferrite solid solutions, crystals were obtained by slow cooling from the melt. These were studied by single-crystal XRD techniques (Weissenberg, precession) to establish the unit cell parameters and assist in the indexing of the powder patterns.

A study was made of sodium loss by volatilization from the silica-free composition $NaFeO_2$, at temperatures between 1000° and 1200°C. At 1000° and 1100°C there was no detectable weight loss after 1 hr. At 1200°C the weight loss was detectable and was monitored at regular intervals over a 27-hr period. The average decrease in weight of the sample was 0.12% per hour.

The DTA studies showed that the positions of the subsolidus phase boundaries were affected by hysteresis and were also dependent on the previous thermal history of the sample. A standard procedure was adopted whereby the prereacted samples were subjected to two DTA controlled heating and cooling cycles, with the first run terminating at temperatures below the solidus line and the second run taken up to the melting point. Approximate liquidus and solidus lines were established beforehand by heating pressed cylindrical pellets and noting the temperatures at which rounding of the sharp edges and slumping of the pellets occurred. The results reported here were taken from the second DTA heating run, for which good thermal contact had been established between the sample and the platinum container.

Results and Discussion

Phase Equilibria

The results of the phase equilibria studies are summarized in Fig. 1. As described in the experimental section, the phase boundaries were determined by a combination of DTA and high-temperature XRD.

As shown in Fig. 1, the β and γ polymorphs of $NaFeO_2$ have a limited solubility for SiO_2. From XRD studies on samples cooled to room temperature, a single phase of the β type was found in compositions with up to 11 mole% SiO_2. The γ-type solid solution could not be quenched to room temperature; high-temperature XRD studies showed that the maximum SiO_2 incorporation was 5 mole% in the tetragonal γ form of $NaFeO_2$. At higher SiO_2 contents, a new orthorhombic phase was stable. We have represented this phase as γ'_{ss}. The lower SiO_2 compositional limit of γ'_{ss} is about 7.5 mole% SiO_2 at a temperature of 1050°C. We have not determined the upper SiO_2 solubility limit in γ'_{ss} precisely, but a few explor-

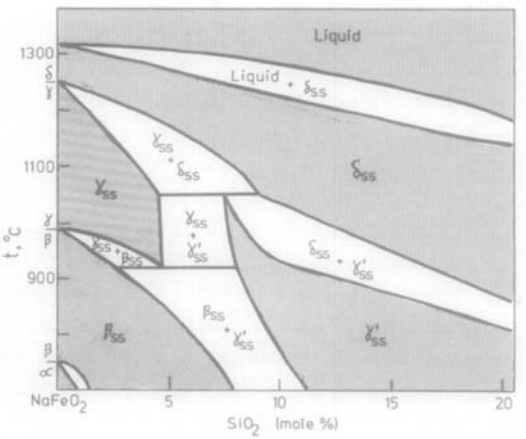

FIG. 1. Phase relations in the system $NaFeO_2$–SiO_2, 0–20 mole% SiO_2, in the temperature range 700–1350°C. The abbreviations are described in the text.

atory runs showed that the solid solution could be prepared for SiO_2 contents up to at least 33 mole%. However, for compositions with more than about 25 mole% SiO_2, hematite and Na_2SiO_3 were always present in the reaction products. The composition with 33.3 mole% SiO_2, i.e., $Na_2O : Fe_2O_3 : SiO_2$, 1–1–1, is very close to the 6–4–5 phase reported by Bowen, Schairer, and von Willems (*3*) in their studies on the system Na_2SiO_3–Fe_2O_3–SiO_2. When we reacted the 6–4–5 composition in the temperature range 700–900°C, we obtained a mixture of γ'_{ss}, Na_2SiO_3, and Fe_2O_3.

The γ'_{ss} solid-solution series could be quenched to room temperature for compositions with greater than 13 mole% SiO_2. An XRD study on quenched samples showed that γ'_{ss} has an orthorhombic superstructure with $a_{\gamma'} \simeq a_\gamma$, $b_{\gamma'} \simeq 2b_\gamma$ and $c_{\gamma'} \simeq 2c_\gamma$. The XRD results will be discussed in the following section.

In addition to the known β and γ polymorphs of $NaFeO_2$, we identified a new cubic polymorph, stable above 1250°C, which we have designated as δ-$NaFeO_2$. The δ phase forms a solid-solution series with SiO_2 (high-cristobalite form) which extends beyond the range reported here, up to at least 33 mole% as evidenced from the exploratory runs on the extension of γ'_{ss} mentioned above. The cubic phase was stable at temperatures up to the solidus line for all compositions, with the lower temperature stability limit decreasing rapidly from 1250°C at 0% SiO_2 to 840°C at 20% SiO_2.

XRD Studies and Crystal Chemistry

(*i*) β_{ss} *Series*

Least-squares refinement of the unit cell parameters for the β solid-solution series was carried out for quenched single-phase products containing 0–11 mole% SiO_2. The results are given in Table I. The parameters

TABLE I

ROOM-TEMPERATURE UNIT CELL PARAMETERS FOR MEMBERS OF THE β AND γ' SOLID SOLUTIONS SERIES[a] IN THE SYSTEM $NaFeO_2$–$xSiO_2$

x	Mole% SiO_2	a (Å)	b (Å)	c (Å)
0	0 (β)	5.671(1)	5.383(1)	7.144(1)
0.05	4.8 (β)	5.636(1)	5.374(1)	7.161(2)
0.075	7.0 (β)	5.608(1)	5.368(1)	7.176(3)
0.125	11.1 (β)	5.571(4)	5.360(2)	7.193(6)
0.15	13.0 (γ')	5.387(2)	10.770(5)	14.641(3)
0.175	14.9 (γ')	5.385(1)	10.771(2)	14.645(2)
0.225	18.4 (γ')	5.377(1)	10.749(2)	14.608(2)
0.275	21.6 (γ')	5.370(1)	10.736(2)	14.574(3)

[a] The β phases were quenched from 1000°C and the γ' phases were quenchd from 800°C.

b_β and c_β have been interchanged relative to the reported (*4*) values (corresponding to a space group setting change from $Pna2_1$ to $Pn2_1a$) to allow a direct comparison with the tetragonal γ phase and the γ' phase. There is a slight decrease in b_β, a larger decrease in a_β, and an increase in c_β with increase in SiO_2 content. Extrapolation of the linear plots of a_β and b_β versus composition gives a point of intersection at about 30 mole% SiO_2. The ratio c_β/a_β at this composition is 1.38, compared with the ideal value of 1.414 ($\sqrt{2}$) for an F-centered cubic cell, described in terms of the equivalent I-centered tetragonal cell.

(*ii*) $\beta_{ss} \rightarrow \gamma_{ss}$ *Transformation*

The change in unit cell parameters as a function of increasing temperature was studied for the β_{ss} and γ_{ss} phases at the upper and lower composition limits for the γ_{ss} series, i.e., at 0 and 5 mole% SiO_2. The results of the unit cell refinements are given in Table II. Indexed diffraction data obtained for the β and γ phases of $NaFeO_2 \cdot 0.05SiO_2$ near the transformation temperature are given in Table III. With increasing temperature the a_β parameter remains essentially unchanged whereas both b_β and c_β increase. At the transformation tempera-

TABLE II

VARIATION OF UNIT CELL PARAMETERS WITH TEMPERATURE FOR THE β AND γ PHASES OF $NaFeO_2$ AND $NaFeO_2 \cdot 0.05SiO_2$

Temperature (°C)	$NaFeO_2$			$NaFeO_2 \cdot 0.05SiO_2$		
	a (Å)	b (Å)	c (Å)	a (Å)	b (Å)	c (Å)
		β phase			β phase	
25	5.671(1)	5.383(1)	7.144(1)	5.636(1)	5.374(1)	7.161(2)
600	5.672(4)	5.424(3)	7.261(8)	5.634(4)	5.419(4)	7.267(6)
700	5.667(3)	5.431(3)	7.378(7)	5.643(5)	5.426(4)	7.307(6)
800	5.664(4)	5.444(3)	7.292(8)	5.628(5)	5.442(5)	7.316(7)
900	5.674(2)	5.461(2)	7.337(3)	5.629(4)	5.450(4)	7.352(5)
					γ phase	
940	—	—	—	5.591(2)	5.591(2)	7.348(3)
980	5.665(5)	5.464(5)	7.353(7)	—	—	—
		γ phase				
1000	5.602(4)	5.602(4)	7.339(8)	5.598(4)	5.598(4)	7.363(6)
1050	5.619(3)	5.619(3)	7.366(4)	5.617(3)	5.617(3)	7.370(4)
1100	5.619(4)	5.619(4)	7.370(6)	—	—	—

TABLE III

X-RAY POWDER DIFFRACTION DATA FOR $NaFeO_2 \cdot 0.05SiO_2$ AT 900°C (β PHASE) AND 940°C (γ PHASE)[a]

	β phase 900°C			γ phase 940°C		
$h\,k\,l$	d_{obs} (Å)	d_{calc} (Å)	I	d_{obs} (Å)	d_{calc} (Å)	I
1 0 1	4.457	4.469	43	4.449	4.450	100
0 1 1	4.389	4.382	57			
1 1 1	3.460	3.459	10	3.482	3.482	17
1 0 2	3.082	3.080	35	3.073	3.071	56
2 0 0	2.814	2.817	35	2.795	2.796	79
0 2 0	2.724	2.727	55			
1 1 2	2.682	2.682	100	2.692	2.692	80
2 1 0	2.502	2.503	10	2.500	2.501	15
1 1 3	2.073	2.079	5	2.081	2.082	12
2 1 2		2.068		2.067	2.067	14
1 2 2	2.042	2.042	11			
2 2 0	1.960	1.958	8	1.978	1.977	11
2 0 3	n.o.[b]	—		1.841	1.842	14
0 0 4	1.839	1.839	16	1.838	1.837	12
3 1 1	n.o.	—		1.719	1.719	12
3 0 2	1.673	1.673	12	1.663	1.662	20
0 3 2	n.o.					
3 1 2	1.599	1.600	4	1.593	1.593	9
1 3 2	1.566	1.566	17			
2 0 4	1.542	1.541	10	1.536	1.535	11
0 2 4	1.526	1.525	13			

[a] Unit cell parameters given in Table II.
[b] n.o. = No observation.

ture, there is a discontinuity in the a_β and b_β cell parameter changes as illustrated for the case of the silica-free phase in Fig. 2. The c_β parameter only changes slightly through the transition region, whereas there is a marked increase in b_β and a decrease in a_β as they merge abruptly to give $a_\gamma = b_\gamma$ of the tetragonal high-temperature phase. At the transformation temperature the c_γ/a_γ ratio is 1.31 for both 0 and 5% silica incorporation. It is interesting to note from Tables I and II that the a_β parameter, which shows negligible change with temperature, is the most sensitive parameter to changes in the SiO_2 content.

The β to γ transformation in $NaFeO_2$ has been studied by West (*10*). He noted that both structures can be described in terms of a distorted hexagonal close packing of anions, with ordering of the Na and Fe atoms in different sets of tetrahedral sites. West proposed a topotactic mechanism for the transformation $\beta \rightarrow \gamma$ involving a coopera-

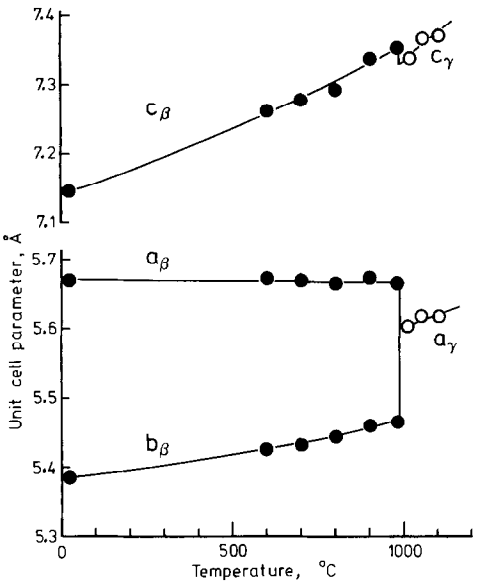

FIG. 2. Variation of unit cell parameters as a function of temperature for the β and γ phases of $NaFeO_2$.

tive displacement (along $[010]_\beta$) of half of the Na and Fe atoms, through their tetrahedral bases, into adjacent tetrahedral sites.

Alternatively, the mechanism for the $\beta \rightarrow \gamma$ transformation can be considered in terms of rotation of the framework of corner-linked FeO_4 tetrahedra using an extension of the structural concepts presented by O'Keeffe and Hyde (*11*). This is illustrated in Fig. 3, in which the structures of both the β and γ forms of $NaFeO_2$ are viewed along [100]. In Fig. 3a it is seen that the β phase contains zigzag chains of corner-linked FeO_4 tetrahedra along [010] with the tetrahedral apices alternately pointing up and down. Successive [010] chains of tetrahedra along [001] are centered at $x \simeq 0$ and $\frac{1}{2}$, respectively. If the FeO_4 tetrahedra in alternate [010] chains (e.g., those centered at $x \simeq 0$) are cooperatively rotated around [100] axes by approximately 40°, as shown by the arrows in Fig. 3a, then the β phase transforms to the γ phase, as shown in Fig. 3b. This mechanism, in contrast to that proposed by West (*10*), does not require Fe–O bonds to be broken and remade. Instead only one Na–O bond per NaO_4 tetrahedron is broken and reformed, changing the linking between the NaO_4 tetrahedron and associated FeO_4 tetrahedra from corner-sharing to edge-sharing. Whereas the mechanism proposed by West involves displacements of cations along b_β, with little change to the anion arrangement, the rotation model involves large movements of the anions in the *bc* plane, with only small associated cation displacements. It should be possible to distinguish between the two mechanisms from a study of the anisotropic thermal vibration parameters of the anions and cations at temperatures close to the transformation temperature. We plan to carry out structure refinements using high-temperature intensity data to investigate this possibility.

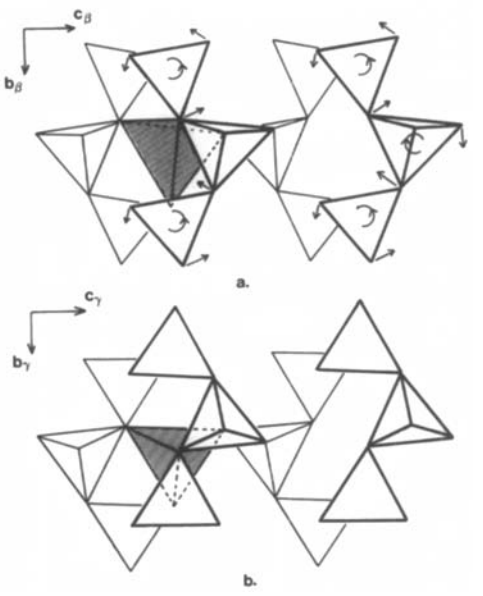

FIG. 3. The structures of (a) β-$NaFeO_2$ and (b) γ-$NaFeO_2$ viewed along the *a* axis of both. The FeO_4 tetrahedra centered at $x \simeq 0$ and $\frac{1}{2}$ are represented by light and heavy lines, respectively. For clarity, only one NaO_4 tetrahedron is shown, with shading. Arrows show the sense of rotation of the FeO_4 tetrahedra and the movement of the oxygen atoms involved in the β to γ transformation.

(iii) The γ'_{ss} Series

Crystals of members of the γ'_{ss} solid solution were obtained by slow cooling from the liquid. Precession and Weissenberg photographs showed an arrangement of intense diffraction spots that could be indexed with a tetragonal cell similar to that for the γ_{ss} phase, i.e., $a \simeq 5.4$, $c \simeq 7.3$ Å, together with weaker reflections that could be indexed with a tetragonal superlattice having doubled tetragonal subcell a and c axes. It was observed that all superlattice reflection indices were of the type $(n, 2n, l)$ and $(2n, n, l)$, n an integer. Thus the patterns could alternatively be indexed in terms of two twin

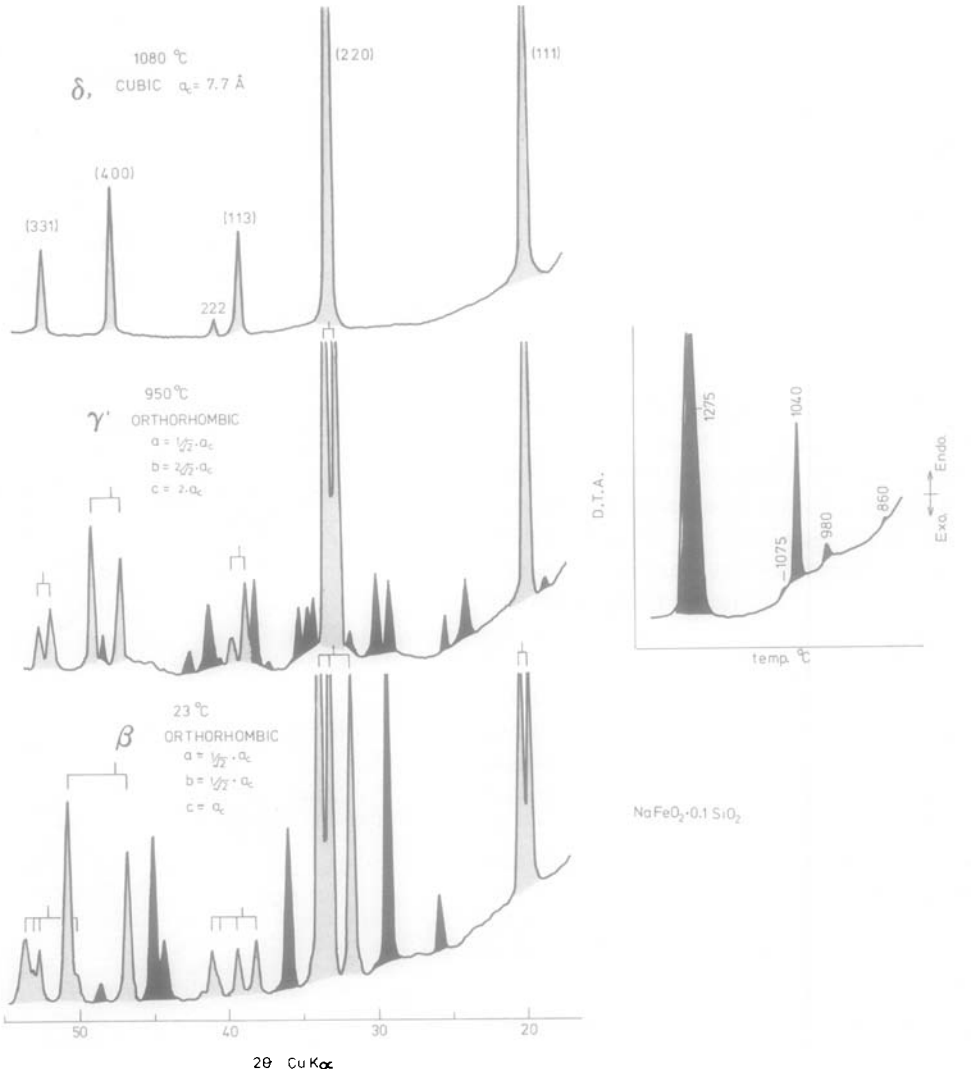

FIG. 4. Powder X-ray diffraction patterns for the β, γ', and δ polymorphs of $NaFeO_2 \cdot 0.1SiO_2$. The face-centered cubic reflections and their equivalents in the β and γ' phases are shaded grey whereas extra reflections due to ordering in the lower-temperature phases are shaded black. The DTA curve for $NaFeO_2 \cdot 0.1SiO_2$ is shown on the right.

variants of an orthorhombic cell, in which only one of the tetragonal subcell axes is doubled, as in the compound $KGaO_2$ (*12*). This situation, in which a lower-symmetry unit cell conforms metrically to one of higher symmetry, occurs commonly when there is a transformation from a high-temperature disordered phase to a low-temperature ordered phase and microdomain formation occurs (*13*). In the case studied here, the γ'_{ss} phase derives from the high-temperature disordered cubic γ_{ss} solid solution. The close relationship between the diffraction patterns of δ_{ss} and γ'_{ss} (and β_{ss}) is shown in Fig. 4. The splitting of the F-centered cubic subcell reflections on passing from δ_{ss} to γ'_{ss} is illustrated, together with the appearance of the superlattice reflections in γ'_{ss}.

TABLE IV

ROOM-TEMPERATURE X-RAY POWDER DIFFRACTION DATA FOR $NaFeO_2 \cdot 0.175SiO_2$ γ' PHASE

h k l	d_{obs} (Å)	d_{calc} (Å)	*I*
1 1 1	4.571	4.575	2
1 0 2, 0 2 2	4.339	4.339	100
1 1 2	4.022	4.024	1
1 0 3, 0 2 3	3.613	3.617	10
1 1 3	3.428	3.429	8
1 2 3	3.002	3.002	12
1 1 4	2.915	2.915	13
1 3 2	2.766	2.766	3
2 0 0, 0 4 0	2.692	2.693	65
1 2 4	2.638	2.639	53
1 0 5, 0 2 5	2.572	2.573	9
1 3 3	2.547	2.548	6
1 1 5	2.501	2.503	4
1 2 5	2.320	2.322	9
1 4 2, 2 2 2	2.288	2.288	5
1 0 6, 0 2 6	2.224	2.223	1
1 3 5	2.091	2.091	2
2 4 0	1.904	1.904	8
1 4 5, 2 2 5	1.860	1.860	2
0 0 8	1.831	1.831	10
3 0 2, 0 6 2	1.743	1.743	2
1 6 3, 3 2 3	1.607	1.608	5
2 4 5 3 3 1	1.596	1.596 1.596	7
1 4 7, 2 2 7	1.579	1.579	2
1 6 4, 3 2 4	1.545	1.544	6
2 5 4	1.528	1.528	4
2 0 8, 0 4 8	1.515	1.514	11

TABLE V

VARIATION OF UNIT CELL PARAMETERS WITH TEMPERATURE FOR THE γ' AND δ PHASES OF $NaFeO_2 \cdot 0.125SiO_2$

Temperature (°C)	*a* (Å)	*b* (Å)	*c* (Å)
25[a] (γ')	5.375(5)	10.75(1)	14.62(1)
700[a] (γ')	5.429(7)	10.86(1)	14.82(1)
800[a] (γ')	5.454(8)	10.91(2)	14.86(1)
900 (γ')	5.475(10)	10.95(2)	14.98(2)
1000 (δ)	7.688(3)		
1060 (δ)	7.689(6)		

[a] Minor β phase present.

The single-crystal diffraction patterns were used to index the powder patterns. An example of an indexed pattern for the γ' polymorph of $NaFeO_2 \cdot 0.175SiO_2$ is given in Table IV. Refinement of the θ values from powder patterns for γ'_{ss} phases quenched from 800°C to room temperature gave the unit cell parameters reported in Table I. As the SiO_2 content is increased from 13 to 21.6 mole%, there is a gradual decrease in all three parameters, in contrast with the β_{ss} solid solution, for which c_β increases with increasing SiO_2 content.

The variation of unit cell parameters with increasing temperature, through the $\gamma' \rightarrow \delta$ transformation, is given for the composition $NaFeO_2 \cdot 0.125SiO_2$ in Table V. The $c_{\gamma'}/a_{\gamma'}$ ratio increases from 1.358 to 1.368 from room temperature to the transformation temperature. These values are about halfway between the corresponding ratios for the γ phase (Table II) and the δ phase (in the equivalent I-centered tetragonal cell representation), suggesting that the structure of the γ' phase may be based on an intergrowth of the γ- and δ-type structures. In further studies we plan to determine the structure of the γ' phase.

(iv) The δ_{ss} Series

In this study we report for the first time a high-temperature cubic polymorph of Na FeO_2, with a transformation temperature $\gamma \rightarrow \delta$ at 1250°C. Because of the high rate of evaporation of sodium from the surface of $NaFeO_2$ above 1200°C, with consequent melting of the iron-enriched compositions, it was very difficult to obtain XRD data for a lattice parameter determination. Eventually, by rapid heating of the sample to 1250°C and immediate recording of the positions of some reflections, a refined unit cell parameter was obtained, using platinum as an internal standard. This gave a_δ = 7.71(1) Å.

The δ_{ss} solid solution extends over the full range of SiO_2 contents studied here, 0–20 mole%. Refinements of the 2θ values obtained at 1080°C for $NaFeO_2 \cdot 0.075SiO_2$ and at 1000°C for $NaFeO_2 \cdot 0.125SiO_2$ gave a_δ parameters of 7.709(5) and 7.688(3) Å, respectively.

Application to the DARS Process

As described in the Introduction, the DARS process involves roasting of spent paper-pulp liquor with hematite at about 1000°C to form sodium ferrite, which is then hydrolyzed in hot water to regenerate fresh NaOH solution. The process is expected to operate with excess iron oxide, corresponding to an Fe/Na molar ratio of about 1.5. Australian natural hematite feedstocks, available in a suitable particle size range for the fluid-bed operation, contain typically about 2.5 to 4 wt% SiO_2 impurity, mainly as quartz. We have found from laboratory experiments that this SiO_2 is incorporated into the sodium ferrite phase only. Assuming complete reaction of 4 wt% SiO_2, this gives a silica-containing ferrite phase of composition $NaFeO_2 \cdot 0.083SiO_2$. From Fig. 1 it is seen that this composition at 1000°C forms a γ'_{ss} phase, which reverts to a β_{ss} phase on cooling to room temperature. For hematite feedstocks containing more than about 4 wt% SiO_2, treated under the same conditions as above, the δ phase will be formed and revert to the γ' phase, then the β phase. For SiO_2 contents greater than about 7 wt% the γ' phase will be retained on cooling. At APPM, laboratory testing of the DARS process was carried out using various hematite feedstocks with SiO_2 contents ranging from 0.17 to 7.3 wt%. The residual Na_2O remaining in the hydrolysis product showed a direct linear relationship to the amount of SiO_2 in the hematite. For a hematite with 4% SiO_2, 40% of the original sodium remained in the hydrolysis product, and for a hematite with 7.3% SiO_2, almost 70% of the sodium was unattacked during hydrolysis. On recycling the iron oxide to the roaster, APPM found that subsequent additions of sodium are essentially fully released. XRD patterns for the roast product from those two samples showed β and γ' ferrites, respectively, as expected from Fig. 1. The linear relationship between unattacked Na_2O and SiO_2 suggests that both β and γ' structure types retain sodium in a similar way during hydrolysis. A full understanding of the mechanism for sodium retention requires an understanding of the sodium and silica distributions in both the β and γ' phases. Structural studies on these phases are in progress.

Acknowledgments

We thank Mr. A. Bennett and Mr. H. Wunder of APPM for supplying samples from DARS process tests and for helpful discussions. We also thank Dr. J. D. Hamilton for use of the DTA equipment and Mr. I. Madsen for help with the high-temperature XRD experiments.

References

1. G. H. Covey, *Pulp and Paper, Canada* **83,** 92 (1982).

2. K. N. MADDERN, TAPPI 1985 International Chemical Recovery Conference, Prvc: 227 (1985).
3. N. L. BOWEN, J. F. SCHAIRER, AND H. W. VON WILLEMS, *Amer. J. Sci.* **20,** 405 (1930).
4. D. W. COLLINS AND L. N. MULAY, *J. Amer. Ceram. Soc.* **53,** 74 (1970).
5. M. S. GOLDSZTAUB, *Compt. Rend.* **196,** 280 (1933).
6. F. BERTAUT AND P. BLUM, *Compt. Rend.* **239,** 429 (1954).
7. R. COLLONGUES AND J. THERY, *J. Bull. Soc. Chim. Fr.,* 1141 (1959).
8. J. THERY, *Ann. Chim.* **7,** 207 (1962).
9. J. THERY, A. M. LEJUS, D. BRIANGON, AND R. COLLONGUES, *Bull. Soc. Chim. Fr.,* 973 (1961).
10. A. R. WEST, *Nature (London)* **249,** 245 (1974).
11. M. O'KEEFFE AND B. G. HYDE, *Acta Crystallogr., Sect. B* **32,** 2923 (1976).
12. E. VON VIELHABER AND R. HOPPE, *Z. Anorg. Allg. Chem.* **369,** 14 (1969).
13. M. LABEAU, I. E. GREY, J. C. JOUBERT, J. CHENEVAS, A. COLLOMB, AND J. C. GUITEL, *Acta Crystallogr., Sect. B* **41,** 33 (1985).